

# Magnetic Resolver Using Linear Hall-Effect Sensors

Ye Gu Kang  
Electrical & Electronic Dept.  
Koreatech.  
kang@koreatech.ac.kr

David Reigosa  
Electrical & Electronic Dept  
University of Oviedo  
Gijon, Spain  
diazdavid@uniovi.es

Diego F. Laborda  
Electrical & Electronic Dept.  
University of Oviedo  
Gijón, Spain  
dlaborda@uniovi.es

Fernando Briz  
Electrical & Electronic Dept  
University of Oviedo  
Gijón, Spain  
fernando@isa.uniovi.es

Daniel Fernández  
Electrical & Electronic Dept.  
University of Oviedo  
Gijón, Spain  
fernandezalodaniel@uniovi.es

## Post Conference Paper

**Abstract**— Precise measurement/estimation of rotary position is essential for the control of AC electric machines. Accurate measurement of angular position in industry applications is typically accomplished using encoder and resolvers. Variable reluctance (VR) resolvers are a well-suited option because of their inherent robustness in harsh environments; however, they occupy a substantial percentage of the total drive cost. This paper presents a novel magnetic resolver using low-cost linear Hall-effect sensors. A series of design optimization processes proposed a corresponding prototype evaluated both by finite element analysis (FEA) and subsequent experiments. Two alternative mechanical designs are discussed: shaft and in-shaft types. The proposed magnetic resolver possesses the advantages of conventional encoders including compactness and a reduced manufacturing costs, while maintaining the advantages of VR resolvers. Also, the sensor is fully compatible with conventional drives in electrical terms.

**Keywords**—Magnetic Resolver, Hall-sensor, angular position measurement, angular position measurement.

## I. INTRODUCTION

Electric drives are used in a large variety of applications, including domestic, industrial, traction, aerospace, etc. Precise control of AC electric machines can be achieved by accurate measurement of the rotary position. Optical encoders (optical-based angular position sensors) and resolvers (inductive-based angular position sensors) are the most used sensors in the industry [1]-[5], but many other alternatives have been reported in the literature; capacitive [2]-[3], inductive [4] or magnetic-based angular position sensors being the most extended. Capacitive-based angular position sensors in [3]-[4] provide high precision output but require additional circuitry to be compatible with standard encoder or resolver signals. Inductive position sensors are axially planar [4], and low weight, with a similar operation principle to a transformer but lack robustness. Magnetic angular position sensors are mainly based on Hall-effect or Giant Magnetoresistance (GMR) devices [16]-[17].

This work was supported in part by the Research, Technological Development, and Innovation Programs of the Spanish Ministry of Economy and Competitiveness, under grant MINECO-17-ENE2016-80047-R and by the Government of Asturias under project IDI/2018/000188 and FEDER funds. This paper was supported by the Education and Research promotion program of KOREATECH in 2022.

commonly used in automotive applications (e.g., throttle position detection, shaft position...) [16]-[17]. Their main drawbacks are the lack of robustness, high inertia, and extra circuitry and space required. Additionally, their performance of accuracy is affected by offset, misalignment, or uniform magnetic flux distribution of the permanent magnets integrated into the rotating part.

In general-purpose applications, optical encoders are the most probable selection, providing incremental or absolute angular position with relatively high precision and noise immunity, but are expensive,extensive

They often exhibit a restricted range of operating temperature and a lack of capability to endure shock and vibration in contrast to resolvers.

Resolvers inherently provide the absolute position with credible precision in various circumstances: high vibration, shock, an extensive region of operating temperatures, and high speed of rotation. Resolvers can be brushless wound field (WF) [8], brushed (in disuse), or variable reluctance (VR) [9]-[10]. A brushless resolver is a rotary transformer, whose primary windings are stationary and secondary windings rotate, excited by AC voltage to maintain magnetic coupling with the rotor winding even at a standstill [8]. An AC voltage is induced in the output winding (stator), modulated by the rotor position. Brushes or rotary transformer is needless since VR resolvers include the output and the excitation windings in the stator without rotor windings and bearings. VR resolvers can be frameless mounted and combined into the motor without a coupling device and additional friction to the system [7], making them attractive in traction applications (i.e., electric vehicles and hybrid electric vehicles), [7]-[8]. However, the drive cost is the main constraint [6], [11]. A special type of VR resolvers have been recently proposed including permanent magnets (PM) in the stator, i.e., field modulation PM resolvers [19]-[20]. In [19], magnets of ferrite material are inserted in the back iron (stator part) of the resolver to avoid the usage of excitation signals at high speeds. In [20], ferrite magnets integrated into the stator teeth induce variable flux leakage (sinusoidal) due to the variable reluctance property of the rotor, which can be estimated using linear Hall-effect sensors.

삭제함: prediction

삭제함: ary

삭제함: To reach accurate

삭제함: ,

삭제함: are the general preference in the industry

삭제함: re

삭제함: O

메모 포함[백1]: Hyeong-meen Baik

Do conventional encoders include compactness and a reduced cost compared to the resolvers?  
If so, I think the types of encoders should be mentioned or restricted, since there exist various encoders with big sizes or high prices.

삭제함: !

삭제함: s

삭제함: recently

삭제함: is

삭제함: types

This paper proposes an alternative design of a magnetic resolver using **magnetic** field sensors (i.e., linear Hall-effect) and a moving part composed of non-laminated electrical steel and permanent magnets [24]. In contrast to the VR resolver, the **proposed** design is simpler, more compact, cheaper, and easier to be manufactured; it requires neither stator/rotor laminations nor windings, the stator is made of a simple ferromagnetic ring, and the rotor is made of a VR design alike optimized shape but including magnets. The **proposed** **designed** requires the addition of sensors and conditioning electronics. However, its power consumption is **as marginal**. It can also produce more than one independent output for the redundant mode of operation; **duplicated** and separated outputs can be provided where redundancy is needed. The size or the number of poles is easily scalable to meet the requirements of a specific application. Since it maintains the main properties of the VR resolver, fully compatible with standard resolver signals, modification in the cabling or electronics of the drive is not required. This paper also describes the optimization process of composing the resolver geometry, an FEA of the system, and the experimental validation.

The paper is organized as follows: Section II proposes principle of operation, section III discusses rotor design optimization of the suggested magnetic resolver, and Section IV presents the validation of the corresponding model by means of FEA. An assembly of the proposed prototype is displayed in section V. Following Experimental results and conclusions are presented in sections VI and VII, respectively.

## II. PRINCIPLE OF OPERATION

A brief description of conventional resolvers intended to establish the basis for estimation of the suggested model is presented below.

Resolvers can be broadly classified into two types: brushless wound field (WF) and variable reluctance (VR). Voltage in the rotor winding of WF resolvers is induced by an AC voltage, which is the result of a magnetic coupling (i.e., brushless WF, see Fig. 1a). When it comes to the stator winding, voltages are **sine** and **cosine** signals due to the modulation by the rotor position  $\theta_r$ . Windings of VR resolvers, in contrast, operates as the excitation and outputs (see Fig. 1b), without the use of brushes or slip rings. In addition, they can be in-shaft installed. As an AC voltage/current signal is inserted into the excitation winding, the resulting voltages induced in the stator windings **outputs** are **sine** and **cosine** signals, whose angle is modulated by the rotor angle **similarly** to the WF case. VR resolvers are made simple and robust, which allows a wider operating temperature capacity, less sensitivity to noise, and longer transmission cables [7][8].

Both are a **certain** type of rotary transformer that couples a primary winding (Excitation see Fig. 1) with two secondary windings (**Output 1 & 2**) **with** 90 electrical degrees phase shift. The excitation signal, i.e.,  $v_E(t)$  in Fig. 1, is generally sinusoidal (1) (see Fig. 2a), of magnitude and angular frequency  $E_0$  and  $\omega_s$ , respectively. The output signals of the resolver are  $v_S(t)$  (2) and  $v_C(t)$  (3) (see Figs. 2b and 2c), where  $k$  is the equivalent turns ratio of the magnetic coupling,  $\theta_r$  is

the rotor angle, and  $X$  is a multiplication factor for the angle [6].

$$v_E(t) = E_0 \sin(\omega_s t) \quad (1)$$

$$v_S(t) = E_0 \sin(\omega_s t) k \sin(X\theta_r) \quad (2)$$

$$v_C(t) = E_0 \sin(\omega_s t) k \cos(X\theta_r) \quad (3)$$

$$v'_S(t) = k' \sin(X\theta_r) \quad (4)$$

$$v'_C(t) = k' \cos(X\theta_r) \quad (5)$$

$v_S(t)$  and  $v_C(t)$  are the inputs to a resolver-to-digital (R/D) converter, typically **consisting** of a demodulation stage to **remove** the excitation signal; (4) and (5) are obtained after the demodulation process. A large variety of methods have been reported to obtain the rotor angle,  $\theta_r$ , from (4) and (5) [15], [21]-[23].

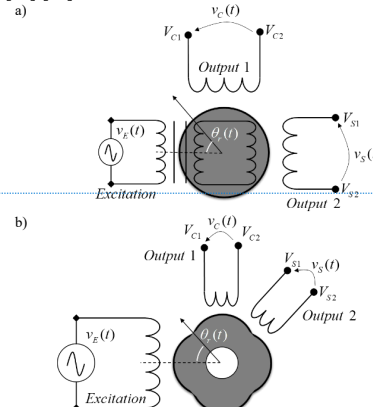
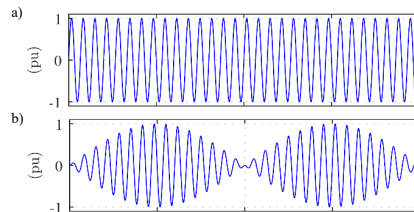


Fig. 1. Schematic representation of resolvers, a) WF and b) VR.

### A. Principle of Operation of the proposed magnetic resolver

The schematic representation of the **proposed** magnetic resolver and the arrangement of linear Hall-effect sensors are shown in Fig. 3. The proposed magnetic resolver consists of a rotor made of a non-laminated ferromagnetic core and permanent magnets. In addition, it includes a stator integrated with two elements of magnetic field measurement, which have a phase difference of 90 electrical degrees. Linear Hall-effect integrated circuit (IC) sensors will be used for the proposed magnetic resolver. These types of ICs allow current control through the Hall-effect element without **additional** electronic **circuits**.



삭제함: suggested

삭제함: Though

삭제함: it

삭제함: ,

삭제함: much lower

삭제함: interpret

삭제함: s

삭제함: R

삭제함: suggested

삭제함: With respect to

삭제함: the winding in the stator

삭제함: winding (see Fig. 1b),

삭제함: age

삭제함: in the same way as for

삭제함: peripheral

삭제함: s

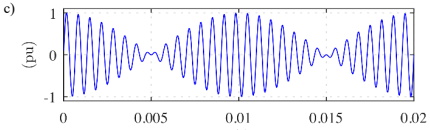


Fig. 2. Normalized signals of conventional resolvers. a) excitation,  $v_e(t)$ , b) Output 1 of the resolver,  $v_1(t)$  (i.e., cosine), c) Output 2 of the resolver,  $v_2(t)$  (i.e., sine).  $\omega_s = 2 \cdot \pi \cdot 500 \text{ rad/s}$ ,  $\omega_r = 2 \cdot \pi \cdot 50 \text{ rad/s}$

Linear Hall-effect sensors generally operate on DC voltage (6) or current input, see Fig. 4a, resulting in a variation of the output voltage of the hall elements, where the differences are phase-shifted voltages  $v_{HS}(t)$  and  $v_{HC}(t)$  (see Fig. 3). For the case of constant rotor speed, corresponding  $v_{HS}(t)$  and  $v_{HC}(t)$  are (7)-(8), see Fig. 4b and Fig. 4c. While these signals are modulated by the angle position of the rotor, they differ from the signals provided by conventional resolvers, where the output signals follow amplitude modulation of the rotary position with the excitation signal as the carrier signal (see Fig. 2). In complement, the Hall-effect sensors can operate on an AC voltage (or current) source. Since the quiescent voltage of the linear hall-effect sensor is proportional to the voltage supply, the variation of the supply voltage input induces the reference output voltage to oscillate as the carrier signal of the amplitude modulation. For the case of fixed rotor speed, the deviation in the output signals of the Hall-effect sensors will be (11)-(12), see Fig. 4d and Fig. 4f, which are equal to the signals provided by conventional resolvers. Note that for every pair of poles (p) in the rotor, four Hall-effect sensors can be installed in the rotor, providing duplicated signals for applications where redundancy is required.

It must be remarked that (11)-(12) results from a sinusoidal flux distribution in the rotor surface. Rotor design to achieve this target is described following.

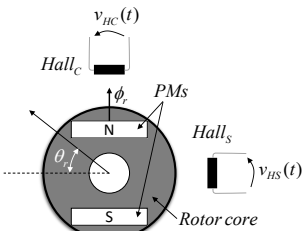


Fig. 3. Schematic representation of the proposed magnetic resolver and position of the Hall-effect sensors.

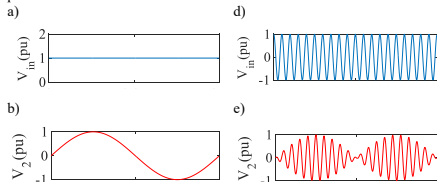


Fig. 4. Excitation and resulting waveforms of the proposed resolver: a) DC excitation, b) Sin output for DC excitation, c) Cos output for DC excitation, d) AC excitation, e) Sin output for AC excitation, f) Cos output for AC excitation.

$$v_E(t) = E_0 \quad (6)$$

$$v_{HS}(t) = k \sin(\theta_r) \quad (7)$$

$$v_{HC}(t) = k \cos(\theta_r) \quad (8)$$

$$v'_{Hall}(t) = k i(t) B(t) \quad (9)$$

$$v_E(t) = E_0 \sin(\omega_s t) \quad (10)$$

$$v_{HS}(t) = E_0 \sin(\omega_s t) k \sin(\theta_r) \quad (11)$$

$$v_{HC}(t) = E_0 \sin(\omega_s t) k \cos(\theta_r) \quad (12)$$

$$MO = \text{Penalty} + \sum^3 O_n w_n \quad (13)$$

### III. ROTOR DESIGN OPTIMIZATION OF THE PROPOSED MAGNETIC RESOLVER

The design optimization process applied to the proposed magnetic resolver is explained in this section. The rotor geometry has been optimized to achieve three main targets:

1. Minimize the use of magnetic materials as it will impact the final economical cost of the system.
2. Reach a desired level of fundamental airgap flux amplitude. This is key as since higher airgap flux densities will increase the signal to noise ration of the output signal of the resolver.
3. Minimize the total harmonic distortion (THD) on the flux density waveform. Low THD values are desired as it will ease the demodulation stage, increasing the dynamics of the resolver as well as its measurement error.

Differential evolution optimization technique [13] was used to find the optimum solution in the design space using 2D finite element analysis (FEA). Rotor parameters are shown in Fig. 4 and Table I.

The desired properties of the Hall-effect sensor-based resolver are included in the objective function variable,  $O_n$ , of the multi-objective (MO) function (13): the total harmonic distortion (THD) of the flux density,  $O_1$ , the magnitude of the airgap flux density,  $O_2$ , and the volume of the permanent magnet (PM),  $O_3$ ; where  $w_n$  is the weighting factor of each objective variable. The fundamental component of the airgap flux density will determine the sensitivity of the proposed resolver, where the THD indicates the quality of the signal for the rotor position estimation. The PM volume is included in the objective function to minimize the system cost, considering the magnetic materials compose a large portion of the total cost. The goal of the multi-objective optimization

메모 포함[백2]: V1 and V2 are not specified in the given schematic Fig.3

메모 포함[DFA3R2]: Right, feel free to change it according to Fig. 4. i will share the matlab script I used to create this representation so you can format the figures.

삭제함: Conventional Resolver

삭제함: nce

삭제함: m

서식 지정함: 글꼴: (영어) Times, 글꼴 색: 텍스트 1

서식 지정함: 글꼴: (영어) Times, 글꼴 색: 텍스트 1

삭제함: .

서식 지정함: 글꼴 색: 자동

삭제함: r

삭제함: the

서식 지정함: 글꼴: (영어) Times, 글꼴 색: 텍스트 1

서식 지정함: 글꼴: (영어) Times

서식 지정함: 글꼴: (영어) Times

삭제함: .

서식 지정함: 글꼴 색: 자동

삭제함: and m

서식 지정함: 글꼴 색: 자동

서식 지정함: 글꼴: (영어) Times, 글꼴 색: 텍스트 1

서식 있음: 들여쓰기: 첫 줄: 0 cm

서식 지정함: 글꼴: (영어) Times

삭제함: I

메모 포함[DFA4]: It would be nice to have a brief explanation why the weights are set to 20, 20000 and 10. Why no other numbers? What is the reason?

메모 포함[백5R4]: The coefficients were decided inductively, which could provide better convergence and results. To provide analytic reason, comparisons of other weighting factors are needed. I think it is out of scope, thus I decided to remove weighting factors in Table 2.

is to find a minimum cost of MO function, (13). More details about the variable used in the multi-objective optimization are in Table II; the penalty is used for eliminating designs that violate the geometric boundary shown in Table I and Fig. 4.

TABLE I. GEOMETRIC PARAMETERS DESCRIPTION

Symbol	Definition
Darc1	Rotor d-axis outer diameter
Darc2	Rotor q-axis outer diameter
ØDhall	Hall sensor distance from the center
ØDim	Rotor inner diameter
ØDring	Ring outer diameter
Ring_th	Ring thickness
Rarc1	Rotor d-axis outer arc
Rarc2	Rotor q-axis outer arc
mtb	Magnet thickness
Min1	Magnet distance from ØDarc1
mgap	Magnet gap in slot
SW	Slot width
Bth1	Outer bridge thickness
Bth2	Inner bridge thickness

TABLE II. PARAMETERS OF THE MULTY-OBJECTIVE FUNCTION

Symbol	Function	Definition
O <sub>1</sub>	THD	Total Harmonic distortion of magnetic flux density in %
O <sub>2</sub>	(B <sub>Hall</sub> - 0.08) <sup>2</sup>	Function of Fundamental magnetic flux density amplitude in Tesla to achieve a target amplitude of 0.08
O <sub>3</sub>	PM Volume	Volume of Permanent magnet in mm <sup>3</sup>
Penalty	0 if within the boundary 100 if outside boundary	Penalty is given when the input parameters are outside the minimum and maximum range.

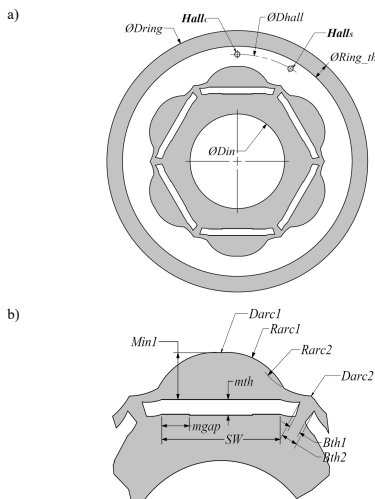


Fig. 4. Dimensions of the magnetic resolver a), general view and b), detailed view of one magnetic pole.

The resulting optimized resolver design will be, therefore, highly sensitive to rotor position, with low harmonic distortion, and low-cost given the pre-defined boundary conditions. Three different types of permanent magnet materials have been evaluated: Ferrite, sintered NdFeB, and bonded NdFeB magnets.

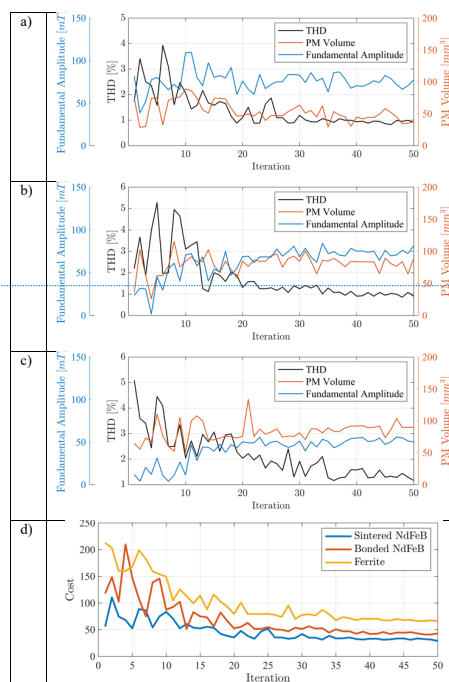


Fig. 5. A series of the optimization process results (total harmonic distortion, permanent magnet volume, fundamental amplitude, and the cost) a) Sintered NdFeB magnets, b) Bonded NdFeB magnets, c) Ferrite magnets, and d) Total cost.

The corresponding results of the optimization process using Differential evolution are shown in Fig. 5. All the records were done through Finite Element Analysis (FEA) simulation. Fig. 5a shows the sequential convergence of sintered NdFeB magnets regarding total harmonic distortion, permanent magnet volume, and fundamental amplitude as iteration increases, while Fig. 5b and Fig. 5c show the cases of bonded NdFeB and Ferrite respectively. Each data point represents the corresponding outputs (i.e., THD, PM volume, and fundamental amplitude) of the least cost solution among the population on the designated generation. Since the magnetic energy product of sintered NdFeB is bigger than that of Ferrite and bonded NdFeB magnets, the permanent magnet volume of Sintered NdFeB is expected to be the smallest for the optimal model. Fig. 5d manifests the total cost, which is the value of the multi-objective function, for the three

삭제함: .

삭제함: I

[1] 이동함(삽입)

[1] 위로 이동함: <#>GEOMETRIC PARAMETERS DESCRIPTION</#>  
Symbol

삭제함: <#>Symbol

삭제함: ↵

삭제함: X

서식 지정함: 강조

삭제함: E

삭제함: X

서식 지정함: 강조

삭제함: As the fundamental amplitude reaches the aimed magnetic flux density, the optimized model can be expected to be sensitive to the angular position of the rotor. Concerning THD, it decreases while iteration increases for whole cases.

permanent magnets as iteration increases. The convergence of the total cost indicates the fundamental amplitude reaches the expected magnetic flux density that could drive the model to be sensitive to the angular position of the rotor while reducing total harmonic distortion.

Fig. 6 shows an example of the flux distribution when using the selected geometry for the three permanent magnet materials. The main properties of each case are shown in Table III. As expected, the maximum peak flux density in the airgap is obtained with the prototype equipped with sintered NdFeB magnets, see Table III. This will allow better use of the measuring range of the Hall-effect sensor, eventually improving the signal-to-noise ratio. To reach a similar peak flux density, bonded NdFeB magnets need almost twice of magnetic material compared to sintered NdFeB, see Table III. Ferrite magnets provide the smallest flux density, with a peak value smaller than the measured peak of NdFeB magnets, which is the expected result considering their magnetic properties. According to the ratio between the fundamental flux amplitude and the volume of permanent magnets, Ferrite magnet volume must be around 3/2 times to achieve the magnetic flux density of NdFeB magnets. Note that the cost function of Fig. Xd represents not the actual cost of the model, but the value of the multi-objective function, (13). Regardless of the objective function and the relatively large volume of the ferrite-based model, the Ferrite magnet will be cheaper than other cases due to the reduced material cost.

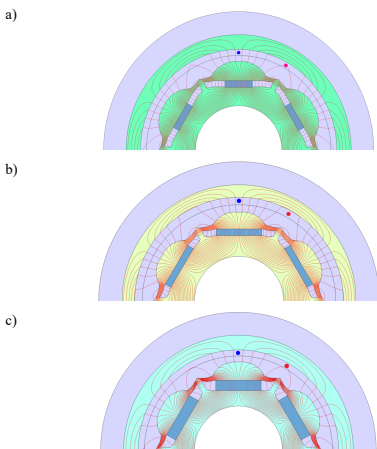


Fig. 6 Flux lines distribution for the optimized magnetic resolver design equipping a) Sintered NdFeB magnets, b) Bonded NdFeB magnets, and c) Ferrite magnets. Blue (●) and red (●) spots represent the Hall<sub>c</sub> and Halls sensors.

TABLE III. OPTIMIZATION RESULTS OF THE MAGNETIC RESOLVER

	PM Material Types		
	Sintered NdFeB	Bonded NdFeB	Ferrite
THD (%)	0.92	1.08	1.28
Fundamental flux density amplitude (mT)	77.27	72.39	56.03
PM volume (mm <sup>3</sup> )	37.16	64.75	103.70

<sup>a</sup> Results obtained from FEA simulation

#### IV. VALIDATION OF THE RESOLVER USING FEA

This section shows FEA results for the three optimized prototypes using sintered NdFeB, bonded NdFeB, and Ferrite, respectively while rotating.

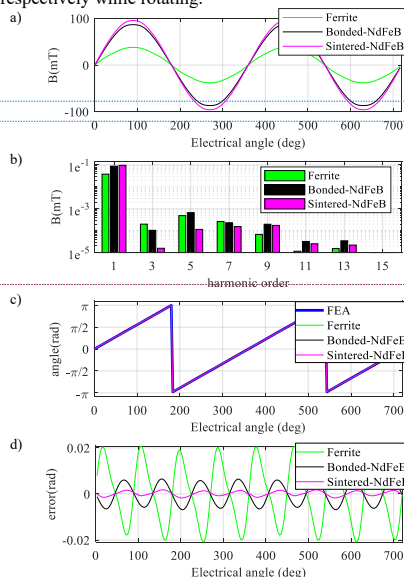


Fig. 7 Performance of the three types of resolvers. a)  $\sin$  output of the hall effect sensors, b) FFT of  $\sin$  output (in a), c) resulting position angle, and d) resulting angle error.

Fig. 7a shows the magnetic flux density at the position of the linear Hall-effect sensor (see Fig. 3 and 5) for one rotor rotation and for the three magnetic materials. Fig. 7b manifests the corresponding Fast Fourier Transform (FFT) outputs, from which the THDs in Table III are obtained. It can be observed that the THD in all cases is <1.55%, all harmonics being at least two orders of magnitude smaller than the fundamental component. It is noted that these results might be influenced by the bandwidth of the Hall-Effect sensors, which is typically >250kHz [12]; i.e., the bandwidth of the Hall-effect sensors will have virtually no influence on standard machines used in traction applications [14]. Fig. 7c shows the prediction of rotary angle for the three different magnetic materials and the real position. Fig. 7d shows the error in the estimated position; variations in the errors being due to the harmonics in the flux waveform shown in Fig. 7b, i.e., they are not the results of assembling tolerances, circuitry, noise, misalignments, etc.

**메모 포함[DFA6]:** This should be commented for the figures Xa, Xb and Xc since they represents different cases. Please, write this paragraph again trying to explain the behavior or the small differences among the cited cases. A minor comment citing figures one by one is enough. This is a complex part and i think is not properly explained right now.

**삭제함:** The total cost reduction (see Fig. Xd) represents that the optimization process can provide an optimized magnetic resolver model achieving the desired boundary conditions and target conditions for each type of magnet.

**삭제함:** 5

**서식 있음:** 들여쓰기: 첫 줄: 0.63 cm

**삭제함:** desired

**삭제함:** disposition

**삭제함:** smallest

**삭제함:** manufacturing

**서식 지정함:** 글꼴: (영어) Times, (한글) SimSun, 글꼴 색: 빨강

**삭제함:** 6

**삭제함:** 6

**삭제함:** 5

**메모 포함[백7]:** I think that the bandwidth of the Hall-Effect sensors is debatable. The linear Hall-effect sensors that I searched do not follow the given bandwidth.

**메모 포함[DFA8R7]:** This info was provided by the sensors' manufacturer in an email since this info is not given in the datasheet.

**삭제함:** 6

**삭제함:** 6

**삭제함:** 6

It can be observed in Fig. 7d that the lower error is obtained for the sintered NdFeB magnet, while ferrite magnets show the worst behavior. Measurement errors are  $\pm 1.1^\circ$  (Ferrite based),  $\pm 0.35^\circ$  (bonded NdFeB based), and  $\pm 0.09^\circ$  (sintered NdFeB based). Position error of commercially available resolvers is in the range of  $\pm 0.5\text{--}1.0^\circ$  for VR resolvers [11] and around  $\pm 0.16^\circ$  for brushless resolvers, meaning that the accuracy of the proposed system is comparable with commercially available resolvers.

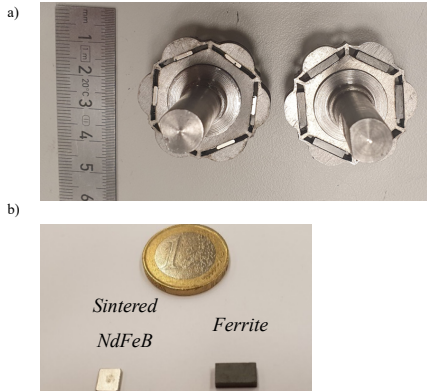


Fig. 8. a) Lamination of the optimized geometries for the magnetic resolver design equipping: sintered NdFeB (left) and Ferrite (right), and b) NdFeB and Ferrite magnets for the designs in Fig. 7a.

## V. ASSEMBLY OF THE PROPOSED PROTOTYPE

The proposed prototype can be assembled in two different configurations: in-shaft mounting and shaft-type for connections through flexible couplings. For any cases, the necessary circuitry is the same, both allowing redundant configuration (i.e., providing duplicated signals). Fig. 8a shows the laser cutout (silicon steel 50H350) of the optimized designs for the prototypes equipping sintered NdFeB magnets and Ferrite magnets, the PM samples being shown in Fig. 8b. The same laser cutout and magnets will be used for both the in-shaft and shaft-type resolvers.

### A. Shaft-type assembly

The shaft-type magnetic resolver is shown in Fig. 9. It is equipped with the rotor cutout and PMs shown in Fig. 7. It was designed with an 8-mm shaft diameter, the diameter of the body and axial dimensions being 52 mm and 17 mm respectively. This design is suitable for the connection through flexible couplings. It can be observed that the PCB integrates four Hall-effect sensors (i.e., two  $Hall_c$  and two  $Hall_s$ ), i.e., it provides redundant output signals. The design also includes two bearings: front and rear cover hosts.

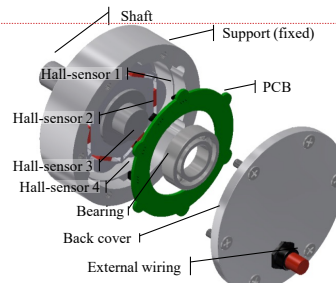


Fig. 9. Disassemble view of the Shaft-type magnetic resolver

삭제함: 6

### B. In-shaft mount assembly

The in-shaft type magnetic resolver is shown in Fig. 10. It is equipped with the rotor cutout and PMs shown in Fig. 8. The rotor of the sensor is directly connected to the machine shaft and fixed by a nut. The axial length of the sensor exploding bolts is 5 mm, and the diameter of the sensor is 70 mm. In this case, the PCB integrates only two Hall-effect sensors (i.e.,  $Hall_c$  and  $Hall_s$ ), although this design also allows redundant configuration. The advantage of this design is that it does not require bearings.

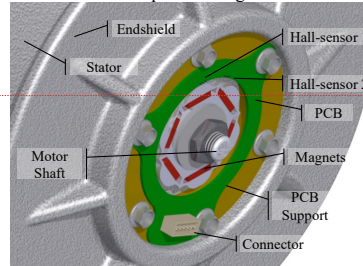


Fig. 10. In-shaft type magnetic resolver inserted in an endshield of a machine.

삭제함: 9

삭제함: 7

삭제함: 7

### C. Electronic circuitry

A conditioning system is required for the proposed prototype to achieve full compatibility with commercial drives in terms of power supply and output voltage levels. Its objective is twofold: provide supply voltages for the Hall elements and the additional ICs and adapt output voltage levels within the range of commercial drives.

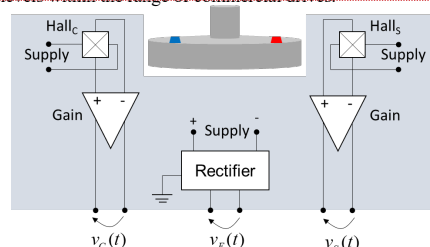


Fig. 11. Simplified representation of the electronic circuitry.

삭제함: 9

삭제함: 7

삭제함: 7

삭제함: 8

삭제함: 0

Fig. 9 shows a simplified representation of the electronic circuit needed for the proposed sensor. The excitation signal, which will be provided by the drive (i.e., standard resolver excitation), is rectified to provide a symmetrical voltage supply to the conditioning circuit, as demanded by operational amplifiers. Hall elements (i.e.,  $Hall_c$  and  $Halls$ ) is supplied by AC voltage which produces AC current through the hall elements since hall elements are resistors from an electrical point of view. Note that a temperature variation of the hall element will directly impact the current through the hall element and therefore, the Hall voltage at its output. However, this will not affect the position measurement since the phase and amplitude of the sine and cosine Hall elements will be exposed to exactly the same conditions given the proximity between them. The rotor position information is embedded in the phase of the current waveforms but not in the amplitude (see Fig. 2).

The total power consumption of the proposed system is in the range of the power consumption of the Hall elements: 12.5 mW per sensor. The power losses due to the rectification stage could be considered as negligible (i.e., conduction losses of a rectified diode). The power consumption of the gain stages could also be considered negligible since ultra-low-power differential operational amplifiers are used. The circuit in Fig. 8 provides differential output signals to enhance noise immunity in the transmission wire.

## VI. EXPERIMENTAL RESULTS

The prototype of the proposed system is shown in Fig. 12 corresponding to the drawing in Fig. 9. The fixed parts of the sensor (i.e., shaft, stator, data acquisition circuitry board, and cover) are shown in Fig. 11a. The assembled system with moving parts (i.e., magnets and rotor shown in Fig. 8) is shown in Fig. 12b. The sensor is attached to a brushless PMSM in a testbench. The prototype integrates two pairs of Hall-effect sensors (i.e.,  $Hall_c$  and  $Halls$ ) for a redundant output, the simplified power and conditioning stages for each pair of sensors being shown in Fig. 11. The prototype has been designed with large tolerances to reduce complexity and ease assembling process.

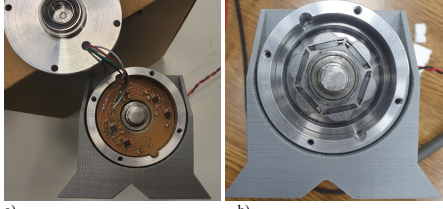


Fig. 12. a) Shaft, stator and data acquisition circuitry board, b) Assembly of proposed resolver.

Fig. 13 shows the output waveforms provided by a pair of Hall-effect sensors (i.e.,  $Hall_c$  and  $Halls$ ) when they are fed with a sinusoidal waveform of  $7V_{RMS}$  at 10 kHz. Fig. 13 shows the simplified signal processing used for speed and position estimation. Measured flux densities by  $Hall_c$  and  $Halls$  are multiplied by the excitation signal,  $V_a$  and  $V_b$  being obtained.  $V_a$  and  $V_b$  normalized, (14), and  $\vec{V}_{dq}$  (15)-(16), is

obtained using a synchronous reference frame phase-locked loop (SRF-PLL), which provides the estimated rotor speed and position [18].

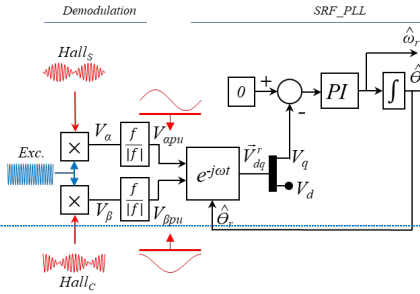


Fig. 13. Schematic representation of the signal processing used for speed and position estimation.

$$V_{\alpha pu} = \frac{V_\alpha}{|V_\alpha|}; \quad V_{\beta pu} = \frac{V_\beta}{|V_\beta|} \quad (14)$$

$$V_{\alpha\beta pu}^s = V_{\alpha pu} + jV_{\beta pu} \quad (15)$$

$$\vec{V}_{dq}^r = V_{\alpha\beta pu}^s e^{-j\theta_r} \quad (16)$$

Fig. 14 shows the experimental results of the assembled resolver using the signal processing scheme in Fig. 13 with the rotor speed of  $250\text{rad/s}$ . The  $V_a$  and  $V_b$  in the demodulation process are shown in Fig. 14a. The output signals from SRF-PLL,  $V_d$  and  $V_q$ , are shown in Fig. 14b. A slight difference between  $V_d$  and  $V_q$  in terms of amplitude can be observed in Fig. 14b due to different radial position of the hall effect sensors in the PCB, see Fig. 11a, due to assembling tolerances.

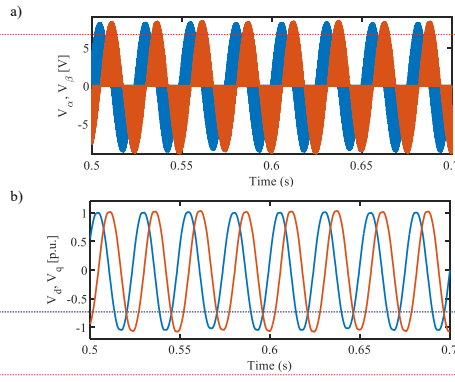


Fig. 14. Magnetic resolver signals,  $\omega_s = 2 \cdot \pi \cdot 10000 \text{ rad/s}$ , or  $= 250 \text{ rad/s}$ .

a)  $V_\alpha$  (red),  $V_\beta$  (blue), b)  $V_d$  (red),  $V_q$  (blue)

Fig. 15 shows the estimated speed and corresponding rotor position obtained from the proposed sensor during dynamic changes of the rotor velocity. The machine rotates

삭제함: 8

메모 포함[백11]: For Fig. 12, I think that after the demodulation part, the output should be the input, sin and cosine, considering the meaning of demodulation. Seemingly, multiplication with exciting signal and following normalization process does not provide the desired output. I concluded that SRF-PLL also takes part in the demodulation process. If I am right, the figure should be revised.

Also, if brief descriptions were added, it would be helpful.

메모 포함[DFA12R11]: I dont get this point. We can have a short discussion on skype or teams.

메모 포함[백9]: Hyeong-been Baik

In this paper, we take the amplitude modulation. Thus, I think the rotor position information affects the amplitude of the carrier signal, not the phase. I think the given sentences are quite ambiguous.

What I understand is below.

If all hall sensors are located at the same temperature, their quiescent voltage and sensitivity would be the same each other, even though the temperature varies. Since it would only influence the gain k in (11), (12), the phase of sine and cosine will be still, which preserves the angular information.

Am I right?

메모 포함[DFA10R9]: Correct, I write it again. Feel free to change it.

서식 지정함: 취소선

서식 지정함: 취소선

서식 지정함: 취소선

삭제함: 2

삭제함: 3

삭제함: 2

삭제함: 1

삭제함: 8

삭제함: 3

삭제함: )

삭제함: 3

삭제함: )

삭제함: 7

삭제함: 3

삭제함: 1

삭제함: 0

삭제함: 1

삭제함: Assembled

삭제함: 2

삭제함: 3

삭제함: 2

삭제함: 4

at 166 rad/s until 1.7 s and decelerated to 0 rad/s until 2.3 s then accelerated to 350 rad/s. Fig. 14b and 14c show the corresponding rotor position and the position error. The maximum position error during transients is 0.165 rad and remains lower than 0.1 rad in steady state.

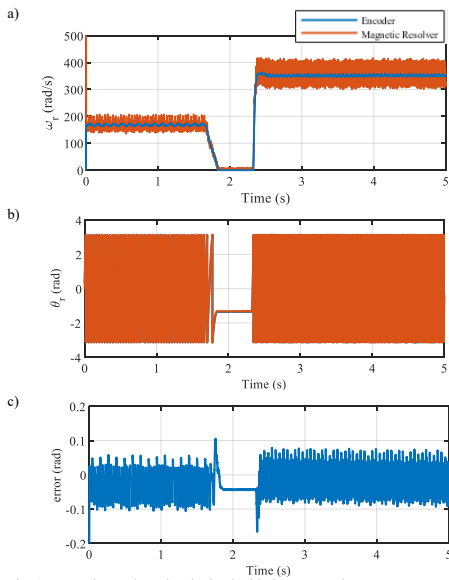


Fig. 15 Experimental results obtained with the proposed sensor,  $\omega_s = 2 \cdot \pi \cdot 10000$  rad/s. a) Speed, b) Angular position, c) Angular position error.

## VII. CONCLUSIONS

A magnetic resolver using Hall-effect sensors is proposed in this paper. Compared to available resolvers, it provides similar accuracy, with a simpler and cheaper construction. Two different designs have been proposed: shaft-type and in-shaft designs; both allowing redundant position measurement. The optimization process of the rotor geometry is shown, and FEA and experimental results have been provided to demonstrate the viability of the proposed system. The experimental results for the prototype show a maximum position error during transients of 0.165 rad that is reduced below 0.1 rad in steady state.

## ACKNOWLEDGMENT

Author would like to thank Bomatec AG for advising and providing magnet samples.

## REFERENCES

- [1] R. M. Kennel, "Why Do Incremental Encoders Do a Reasonably Good Job in Electrical Drives with Digital Control?," Conference Record of the 2006 IEEE Industry Applications Conference Forty-First IAS Annual Meeting, Tampa, FL, 2006, pp. 925-930.doi: 10.1109/IAS.2006.256635
- [2] B. Hou, C. Li, Z. Gao, Q. Wei, B. Zhou and R. Zhang, "Design, Optimization, and Compensation of a High-Precision Single-Excitation Absolute Capacitance Angular Encoder up to  $\pm 4^\circ$ ," in IEEE Transactions on Industrial Electronics, vol. 66, no. 10, pp. 8161-8171, Oct. 2019. doi: 10.1109/TIE.2018.2886762
- [3] H. Pu, H. Wang, X. Liu, Z. Yu and K. Peng, "A High-Precision Absolute Angular Position Sensor With Vernier Capacitive Arrays Based on Time Grating," in IEEE Sensors Journal, vol. 19, no. 19, pp. 8626-8634, 1 Oct., 2019. doi: 10.1109/JSEN.2019.2921479
- [4] M. Howard, Incremental encoders, absolute encoders & pseudo-absolute encoders, Feb. 2013. Accessed on: Dec. 15, 2019. [Online]. Available: [https://www.zettlex.com/wp-content/uploads/2017/08/incremental-encoders-vs.-absolute-encoders\\_Rev\\_3.1.pdf](https://www.zettlex.com/wp-content/uploads/2017/08/incremental-encoders-vs.-absolute-encoders_Rev_3.1.pdf)
- [5] F. Jiang, D. Lou, H. Zhang, L. Tang, S. Sun and K. Yang, "Design of a GMR-based magnetic encoder using TLE5012B," 2017 20th International Conference on Electrical Machines and Systems (ICEMS), Sydney, NSW, 2017, pp. 1-4. doi: 10.1109/ICEMS.2017.8056197
- [6] C. Jin, I. Jang, J. Bae, J. Lee and W. Kim, "Proposal of Improved Winding Method for VR Resolver," in IEEE Transactions on Magnetics, vol. 51, no. 3, pp. 1-4, March 2015, Art no. 8102404. doi: 10.1109/TMAG.2014.2348321
- [7] L. Sun, "Analysis and Improvement on the Structure of Variable Reluctance Resolvers," in IEEE Transactions on Magnetics, vol. 44, no. 8, pp. 2002-2008, Aug. 2008. doi: 10.1109/TMAG.2008.92315
- [8] J. Figueiredo, "Resolver models for manufacturing," IEEE Trans. Ind. Electron., 58(8): 3693-3700, Aug. 2011.
- [9] L. Z. Sun, J. B. Zou, and Y. P. Lu, "New variable-reluctance resolver for rotor-position sensing," in Proc. IEEE Region 10th Conf. TENCON, vol. 4, Chiang Mai, Thailand, pp. 5-8, Nov. 2004.
- [10] H. Saneie, Z. Nasiri-Gheidari and F. Tootoonchian, "Design-Oriented Modeling of Axial-Flux Variable-Reluctance Resolver Based on Magnetic Equivalent Circuits and Schwarz-Christoffel Mapping," in IEEE Transactions on Industrial Electronics, vol. 65, no. 5, pp. 4322-4330, May 2018. doi: 10.1109/TIE.2017.2705862
- [11] T. Suzuki, K. Toyotake and Y. Yamashita, "Variable reluctance type resolver rotor and brushless motor," Japan Patent JP2010048775A, Aug. 25, 2008.
- [12] D. Fernandez et al., "Permanent Magnet Temperature Estimation in PM Synchronous Motors Using Low-Cost Hall Effect Sensors," in IEEE Transactions on Industry Applications, vol. 53, no. 5, pp. 4515-4525, Sept.-Oct. 2017. doi: 10.1109/TIA.2017.2705580
- [13] S. Das and P. N. Suganthan, "Differential Evolution: A Survey of the State-of-the-Art," in IEEE Transactions on Evolutionary Computation, vol. 15, no. 1, pp. 4-31, Feb. 2011. doi: 10.1109/TEVC.2010.2059031
- [14] M. Minowa, H. Hijikata, K. Akatsu and T. Kato, "Variable leakage flux interior permanent magnet synchronous machine for improving efficiency on duty cycle," 2014 International Power Electronics Conference (IPEC-Hiroshima 2014 - ECCE ASIA), Hiroshima, 2014, pp. 3828-3833. doi: 10.1109/IPEC.2014.6870049
- [15] L. Pecl, R. Schindeler, D. Cleveland and K. Hashtrudi-Zaad, "High-Precision Resolver-to-Velocity Converter," in IEEE Transactions on Instrumentation and Measurement, vol. 66, no. 11, pp. 2917-2928, Nov. 2017. doi: 10.1109/TIM.2017.2714378
- [16] P. Kejik, S. Reymond and R. S. Popovic, "Circular Hall Transducer for Angular Position Sensing," TRANSDUCERS 2007 - 2007 International Solid-State Sensors, Actuators and Microsystems Conference, Lyon, 2007, pp. 2593-2596. doi: 10.1109/SENSOR.2007.4300702
- [17] K. Bienczyk, "Angle measurement using a miniature hall effect position sensor," 2009 2nd International Students Conference on Electromagnetic and Mechatronics, Silesia, 2009, pp. 21-22. doi: 10.1109/ISCON.2009.5156096
- [18] D. Reigosa, D. Fernandez, C. González, S. B. Lee and F. Briz, "Permanent Magnet Synchronous Machine Drive Control Using Analog Hall-Effect Sensors," in IEEE Transactions on Industry Applications, vol. 54, no. 3, pp. 2358-2369, May-June 2018. doi: 10.1109/TIA.2018.2802950
- [19] L. Sun, Z. Luo, K. Wang, R. Cao and S. Ding, "A Stator-PM Resolver With Field Modulation Principle," in IEEE Transactions on Energy Conversion, vol. 36, no. 1, pp. 159-172, March 2021. doi: 10.1109/TEC.2020.3001655
- [20] M. Bahari, A. Davoodi, H. Saneie, F. Tootoonchian and Z. Nasiri-Gheidari, "A New Variable Reluctance PM-Resolver," in IEEE

삭제함: [3].

삭제함: .

삭제함: 4

삭제함: a maximum

Sensors Journal, vol. 20, no. 1, pp. 135-142, 1 Jan.1, 2020, doi: 10.1109/JSEN.2019.2941554.

[21] S. Golestan, J. M. Guerrero and J. C. Vasquez, "Single-Phase PLLs: A Review of Recent Advances," in IEEE Transactions on Power Electronics, vol. 32, no. 12, pp. 9013-9030, Dec. 2017, doi: 10.1109/TPEL.2017.2653861.

[22] S. Golestan, M. Monfared, F. D. Freijedo and J. M. Guerrero, "Dynamics Assessment of Advanced Single-Phase PLL Structures," in IEEE Transactions on Industrial Electronics, vol. 60, no. 6, pp. 2167-2177, June 2013, doi: 10.1109/TIE.2012.2193863.

[23] S. Shinnaka, "A Robust Single-Phase PLL System With Stable and Fast Tracking," in IEEE Transactions on Industry Applications, vol. 44, no. 2, pp. 624-633, March-april 2008, doi: 10.1109/TIA.2008.916750.

페이지 4: [1] 삭제함

백형민

2022. 10. 1. PM 4:23:00